

ORBIT modeling of fast particle redistribution induced by sawtooth instability

D. Kim¹, M. Podestà¹, D. Liu², and F. M. Poli¹

¹Princeton Plasma Physics Laboratory, Princeton, NJ 08543, USA

²Department of Physics and Astronomy, University of California, Irvine, CA 92617, USA

January 8, 2018

E-mail: dkim@pppl.gov

Abstract

Initial tests on National Spherical Torus Experiment Upgrade (NSTX-U) device suggest that introducing energy selectivity for sawtooth induced fast ion redistribution is required to improve the agreement between experimental and simulated quantities such as neutron rate and Fast-Ion D-Alpha profiles. The aim of this work is to assess the requirements to properly describe the behaviour of fast ions during sawtooth crash for predictive sawtooth simulations. As the first step, in this work, we use the particle-following ORBIT code to characterize the redistribution of fast particles. In order for a sawtooth crash to be simulated, a spatial and temporal displacement is implemented into the ORBIT code. The perturbation amplitude is determined by comparison with experimental measurement of neutron rate drop. The characteristics of fast ions with different orbit types are investigated in phase and real space. Due to a sawtooth crash, fast ion energy and angular momentum are modified resulting in the redistribution in phase space and orbit type change. The redistribution of fast ions in real space shows that sawtooth instability brings different effect on fast particles with different orbit types as observed in experiments. The initial interpretative TRANSP simulation using the so-called *kick model* based on ORBIT modeling result shows improvement of fast ion redistribution before and after sawtooth crash but the neutron rate still has discrepancy compared to the experimental measurement.

1 Introduction

The sawtooth instability in tokamak plasmas is characterized by periodic fast relaxations of plasma parameters, e.g. electron temperature, followed by a slower recovery in the central region where the safety factor q is below unity [1]. Sawtooth instability generally brings moderate confinement degradation but a sawtooth crash with a long period can lower the β limit by triggering Neoclassical Tearing modes (NTMs) [2], possibly leading to disruption. Sawtooth crashes can also affect the transport of thermal plasma particles and fast ions (e.g. α -particles and particles from auxiliary heating system). The population of particles is redistributed during the crash due to the reconnection of magnetic flux surface. Unlikely to thermal particles, the effect of sawtooth crash on fast ions depends on the characteristic of particle such as energy and orbit type. Therefore, the characteristic of fast ions needs to be taken into account for sawtooth modeling to understand and to interpret quantitatively the experimental results.

After the upgrade from the National Spherical Torus Experiment (NSTX) device [3], NSTX-Upgrade (NSTX-U) [4] is equipped with two neutral beam (NB) injectors, each of which has three sources capable of injecting up to 2.1MW of NB power at maximum energy 95keV. The original NB line from NSTX injects with a deposition profile that is typically peaked on-axis. The second NB line, which was installed as part of the upgrade, is injecting tangentially for off-axis NB current drive. Along with the upgrade of the central solenoid, which resulted in a four-fold increase of the available ohmic flux, the increased available NB power enabled longer pulses on NSTX-U than previously achievable on NSTX [5]. Sawtooth L-mode discharges lasting about 2s were readily obtained during the 2016 campaign, thus providing well-reproducible discharges to investigate sawtooth physics in a spherical torus.

The tokamak transport code TRANSP [6, 7] enables time-dependent integrated simulations of a tokamak discharge. The code can be used to interpret existing experiments, as well as to develop new scenarios or make predictions for future devices (e.g. ITER). The NSTX-U sawtooth discharges can be analyzed using the sawtooth model in TRANSP. The reconnection of magnetic flux surfaces are described using full reconnection [8] or partial/incomplete reconnection model [1] with free parameters such as reconnection fraction for partial reconnection case. For the thermal particles, in an interpretative simulation case, the input profiles already include the effect of sawtooth crash as they are reconstructed at the calculation time step while redistribution of fast ions from NB needs to be described by sawtooth model. For both cases, the sawtooth model is applied for q and poloidal magnetic flux redistribution. A TRANSP simulation including only thermal ion density redistribution by sawteeth results in 50% or larger drop in neutron rate compared the experiment, and brings a question about the effect of fast ions on the neutron rate drops. Another simulation applying the sawtooth model for fast ions can reproduce the experimental neutron rate drops [9].

In order for the TRANSP simulation to match the experimental data, a proper set of free parameters needs to be used. Thus it is difficult to apply the sawtooth model for a predictive simulation since the optimum parameter setting cannot be self-consistently determined. In addition, even though the neutron rate drops can be matched with a free parameter set, other simulation results can be different from the experimental ones. For instance, the distribution of fast ions before and after sawtooth crash obtained from FIDA (Fast Ion D-Alpha) [10, 11] measurement is not consistent with FIDA simulation using required data from TRANSP simulation that match the neutron rate drops [9]. Since the sawtooth model in TRANSP treats fast particles in the same way as thermal particles, the different effect of sawtooth crash on particles with different orbit type and energy cannot be taken into consideration as it is shown in experiments [9] and as introduced in theoretical work [12].

Therefore, in order for the TRANSP simulation to be more quantitative to interpret sawtooth discharges, an improved model to manage the redistribution of fast ion during sawtooth crash needs to be developed. The model is required to take into account the characteristics of fast ion such as energy, toroidal angular momentum and pitch angle that affect the redistribution of fast ions in phase and real spaces. Implementation of such model into TRANSP would enable interpretative sawtooth simulations to validate the model by comparison with experimental measurements from NSTX-U or other conventional tokamaks, not only in terms of neutron rate drop but also for profiles such as fast ion density profile. After that it will be possible to have a more comprehensive predictive model to provide more reliable prediction for fast particle redistribution induced by sawtooth crash beyond simple zero-dimensional theoretical predictions.

In this paper, as the first step, simulations using a Hamiltonian guiding center code ORBIT [13] are carried out. ORBIT simulations can be used as guidance to develop a more comprehensive model for characterizing fast particle redistribution by sawteeth as the dependence of characteristics of fast ion such as orbit types, energy and canonical angular momentum are taken into account in the simulation. A perturbation model implemented into the ORBIT code to represent the sawtooth instability is introduced in Sec. 2 with the experimental scenario of the target discharge. In addition, the comparison with experimentally measured neutron rate drop for the determination of the mode amplitude is discussed. In Sec. 3, the characteristic of fast ion redistribution is investigated for different orbit types and particle energy and initial result of the application of *kick model* [14, 15] based on the ORBIT simulations to TRANSP simulation is shown. Finally, the conclusion follows in Sec. 4.

2 Experimental scenario and simulation methodology

The experimental scenario of the discharge analyzed in this work (NSTX-U #204083 L-mode sawtooth discharge with 1MW injected NB power) is shown in Fig. 1. Plasma current I_p ramps up during about 400ms and remains at 650kA in the flat-top phase. The safety factor profile (q) evolves during the initial current ramp-up and the central value (q_0) reaches unity shortly after the beginning of the current flat-top. As q_0 falls below unity, the signatures of sawtooth activity are clearly seen as repetitive spikes on data from magnetic fluctuation sensors located at the plasma edge on the low-field-side, see Fig. 1e. Repetitive crashes also appear on the central electron density ($n_{e,0}$), temperature ($T_{e,0}$) and neutron rate measurements (Fig. 1c, f), which show measurable drops associated with each sawtooth event. $T_{e,0}$ and $n_{e,0}$ values stay around 1keV and $2 \times 10^{19}\text{m}^{-3}$ during sawteeth activities, respectively. Since the neutron rate is dominated by beam-target reactions, the drops in neutron rate indicate changes of thermal and/or fast ion profiles. Profiles are modulated around quasi-stationary values inside the sawtooth inversion radius, which is located around mid-radius at $R \approx 130$ cm. Since the sawtooth cycles

are the same order of - or shorter than - the sampling rate of the NSTX-U profile diagnostics, e.g. 16ms for Thomson scattering system [16] and 10ms for charge exchange recombination spectroscopy (CHERS) [17], available profile data are re-processed through conditional average to infer the typical recovery rates after a sawtooth event at each radial location. The rates are then used to reconstruct the evolution of profiles on a finer time grid.

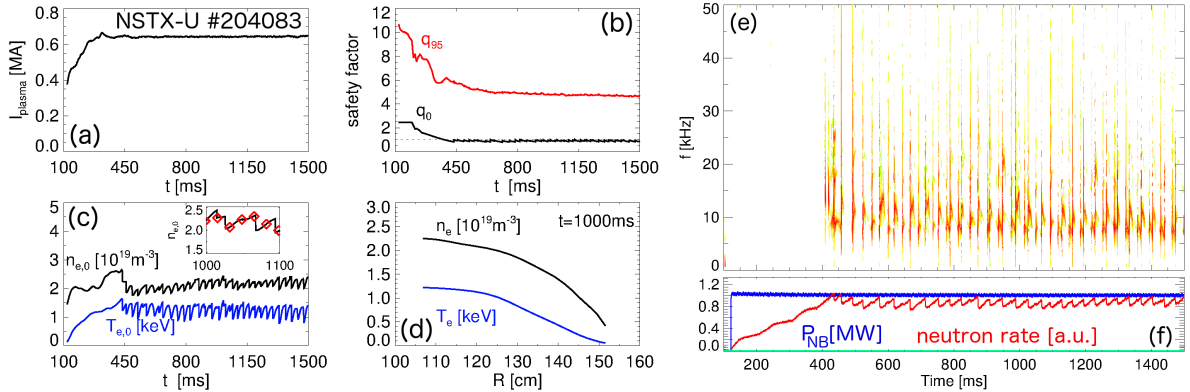


Figure 1: Experimental scenario for NSTX-U discharge #204083. *a*) Plasma current in ramp-up and flat-top phase. *b*) Evolution of central and edge values of the safety factor, as resulting from TRANSP simulation including sawtooth effects on the current profile. *c*) Time evolution of reconstructed central electron density and temperature. The inset shows a subset of reconstructed electron density (solid line) and experimental points (red symbols). *d*) Example of electron density and temperature profiles at $t = 1000\text{ms}$. *e*) Spectrum of magnetic fluctuations from Mirnov coils at the plasma edge. Sawteeth are visible as spikes in the measured spectrum. *f*) Time traces of injected NB power (blue) and measured neutron rate (red).

Simulations have been performed based on the discharge #204083 using the ORBIT code [13], a Hamiltonian guiding-center code for analyzing energetic particle transport by instabilities in tokamaks. The equilibrium from one time slice before sawtooth crash (1093ms) is extracted from an interpretative TRANSP run. The unperturbed initial distribution of 10,000 energetic particles (position, pitch angle and energy) is also extracted from NUBEAM module [18, 19] in TRANSP which calculates the evolution of the energetic particle population based on neoclassical physics. Coulomb collisions, slowing down and charge-exchange events are modeled based on a Monte Carlo approach.

In order to take into account the sawtooth instability, plasma displacement $\vec{\xi}$ has been used to represent the linearized perturbation on the magnetic field,

$$\delta B = \nabla \times (\vec{\xi} \times \vec{B}). \quad (1)$$

The radial component of $\vec{\xi}$ is defined as $\xi(\psi_p, t, \theta, \zeta) = \sum \xi_{mn}(\psi_p, t) \cos(n\zeta - m\theta - \omega t)$, where ξ_{mn} the radial perturbation profile, (m, n) and (θ, ζ) the poloidal and toroidal mode numbers and angles, respectively and ω the mode frequency. The radial profile ξ_{mn} consists of the nominal amplitude $\xi_{0,mn}$, the normalized radial and temporal profiles $\hat{\xi}_{\psi_p, mn}$ and $\hat{\xi}_{t, mn}$. The radial and temporal profiles are taken from Refs. [20, 21] and are shown for (1, 1) mode case in Fig. 2. Since (1,1) mode perturbation can cause a numerical problem to treat the magnetic axis in the ORBITcode, $\hat{\xi}_{\psi_p, mn}$ profile is modified to have zero perturbation at the axis. In addition, the perturbation outside $q = 1$ surface (black dashed line) is set to zero. Note that (1, 1) mode perturbation decreases quickly outside $q = 1$ surface and the modification does not affect much on the simulation result (see Fig. 4).

In NSTX-U, the (1, 1) mode perturbation amplitude typically starts increasing about 1 ~ 2ms before sawtooth crash and the crash duration is typically about 40~50 μs . In this case, the amplitude is set to grow from 10% of the maximum amplitude and sawtooth crash takes place at 1.5ms during 50 μs . Full reconnection is assumed thus after the crash, mode does not survive, i.e. amplitude goes to zero. In the simulation, the amplitude is given by the multiplication of $\xi_{0,mn}$ and $\hat{\xi}_{t, mn}$.

In the ORBIT code, the magnetic perturbation is applied using a scalar function α instead of $\vec{\xi}$ and the perturbed magnetic field is obtained as

$$\delta \vec{B} = \nabla \times (\alpha \vec{B}). \quad (2)$$

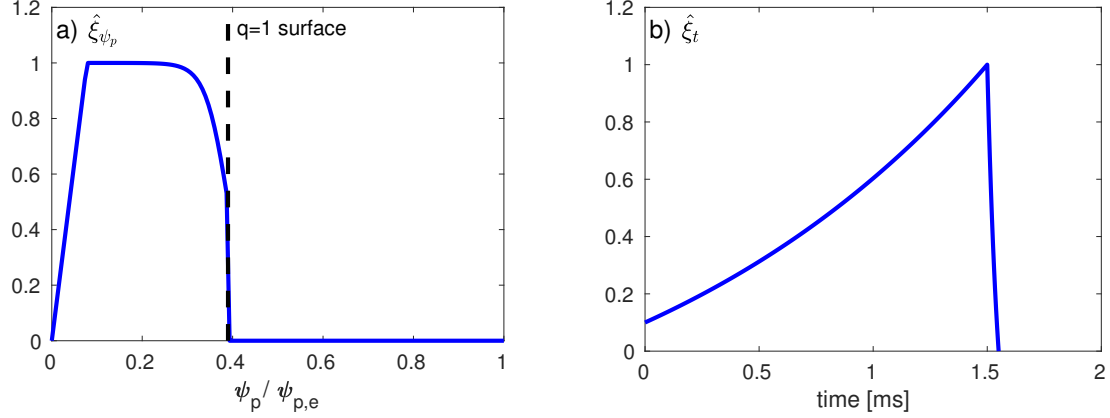


Figure 2: a) Normalized radial displacement $\hat{\xi}_{\psi_p}$ profile. Black dashed line indicates unperturbed $q = 1$ surface. b) Normalized temporal variation $\hat{\xi}_t$ on perturbation amplitude. Sawtooth crash is assumed to happen at 1.5ms during 50 μ s.

Equation (2) brings the perturbed magnetic field equivalent to that from Eq. (1) in radial direction [22]. Since the radial component is the most important in this work and the other components are not used, it is acceptable to use the perturbation from α . Using the relation between α_{mn} and ξ_{mn} (Eq. (3a)), the radial perturbed field is defined as Eq. (3b) [22].

$$\alpha_{mn} = \frac{m/q - n}{mg + nI} \xi_{mn}, \quad (3a)$$

$$\delta \vec{B} \cdot \nabla \psi_p = \sum_{m,n} \frac{mg + nI}{J} \alpha_{mn} \cos(n\zeta - m\theta - \omega t). \quad (3b)$$

The α profile for (1, 1) mode derived from $\hat{\xi}_{\psi_p}$ in Fig. 2a with the perturbation amplitude ξ_0 of 7.5cm is depicted in Fig. 3. The resultant profile has no perturbation at the axis and outside $q = 1$ surface and the curve is similar to a simulation case for TFTR [21].

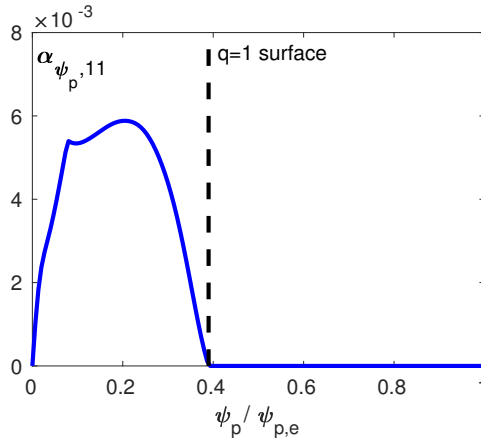


Figure 3: (1, 1) mode radial profile of α converted from $\hat{\xi}_{\psi_p}$ using Eq. (3a). Perturbation is zero at the axis and outside $q = 1$ surface (black dashed line).

The nominal amplitude $\xi_{0,mn}$ is a free parameter in the simulation. Therefore, it is important to take a reasonable value for further analysis. In order to find a proper range, the estimated relative change of neutron rate with different $\xi_{0,mn}$ values is compared with the experimental measurement. Note that neutron rate is relatively well measured in NSTX-U and therefore can reasonably be used for experimental data comparison. The relative change of neutron rate is evaluated using the reaction rate

for D-D reaction, $D + D \rightarrow {}^3\text{He} + n$. The reaction takes place between background thermal deuterium particles and fast particles from deuterium neutral beam injection. The reaction rate is estimated using thermal plasma density n_d from experimental measurement and volume element dV from the ORBIT calculation at each fast particle position, reaction cross section S and square root of energy E of each particle with the given fast ion distribution. The product of those parameters is summed over the number of test particle N and the reaction rate is evaluated for before (subscript 0) and after (subscript f) sawtooth crash, from which the relative change is obtained as seen in Eq. (4).

$$\Delta\text{neut_rate} = \frac{\sum_k^{N_0} n_{d0,k} S_{0,k} \sqrt{E_{0,k}} dV_k - \sum_k^{N_f} n_{df,k} S_{f,k} \sqrt{E_{f,k}} dV_k}{\sum_k^{N_0} n_{d0,k} S_{0,k} \sqrt{E_{0,k}} dV_k}. \quad (4)$$

Using Eq. (4), the relative change of neutron rate induced by (1, 1) mode perturbation is estimated for given amplitudes $\xi_{0,11}$ set between 0.1 and 10cm and the simulation result (blue circle) is displayed in Fig. 4a. The shaded region represents the relative change of neutron rate from the experimental measurement evaluated in the same way as Eq. (4), the difference between the neutron rate at pre- and post-crash divided by the pre-crash neutron rate. Due to the calibration method dependency, the experimental value is given as a range. With smaller mode amplitude, the relative change remains nearly constant as fast particles are not affected much by the perturbation, i.e. the drop is entirely caused by redistribution of thermal ions and the distribution of fast particle does not change as seen in Fig. 4b (blue circle - without perturbation, red cross - application of 1cm perturbation). As ξ_0 increases, fast particles are redistributed by the perturbation (10cm perturbation, green triangle in Fig. 4b) and the relative change of neutron rate increases. The estimated value can be located within the experimental range when the perturbation amplitude is between 5.5 and 9.7cm. For the rest of the analysis, $\xi_0 = 7.5\text{cm}$ has been used.

Note that in the interpretative TRANSP simulation for this discharge the relative change of neutron rate can be larger than the experimental measurements with sawtooth model applying full reconnection for fast ions or be similar or larger without fast ion redistribution induced by sawteeth. This indicates that the conditional average and reconstruction of input profiles for thermal plasma particles may not be accurate enough for sawtooth modeling and/or that the sawtooth model for fast ions is not appropriate either. Therefore, for more reliable sawtoothing discharge simulation, the way to treat input thermal particle profiles and sawtooth driven fast ion redistribution need to be improved.

As briefly mentioned above, the shape of perturbation near $q = 1$ surface does not have a significant effect on the simulation result. The relative change of neutron rate for several amplitude cases are evaluated using the perturbation shape without cutting off the displacement outside the $q = 1$ surface. The result (Fig. 4a red cross) does not change within numerical uncertainties.

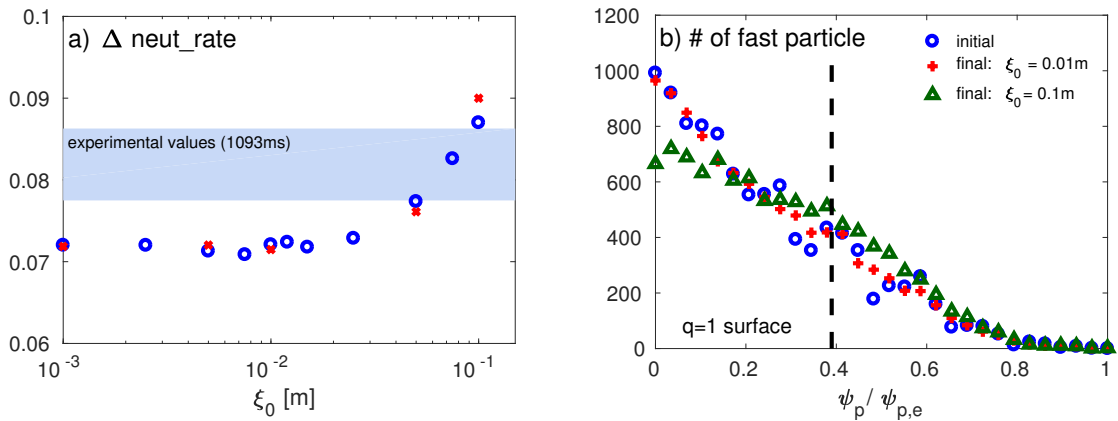


Figure 4: a) The relative change of neutron rate is evaluated using Eq. (4) with different mode amplitude (blue circle). When the mode amplitude is between 5.5 and 9.7cm, simulation result is similar to that from experiment. The result is not sensitive to the perturbation shape. b) With smaller ξ_0 (red cross) fast particles keep the initial distribution (blue circle) while fast particles are redistributed by the perturbation with larger amplitude (green triangle).

3 Simulation result

Using the perturbation shape and amplitude discussed in the previous section, the characteristics of sawtooth induced fast particle redistribution in phase space is investigated in this section. Although the amplitude is determined by comparison with experimental measurement, three different amplitudes ($\xi_0 = 0.1, 1$ and 10cm) are initially used to verify if significant changes are observed in fast particle energy and angular momentum changes induced by the sawtooth crash.

In Fig. 5, initial states of fast particle energy (E) and canonical angular momentum (P_ζ) are shown versus the final states. With the smallest perturbation amplitude (0.1cm , green), E (Fig. 5a) does not change significantly ($\sim 1\%$) while it shows more significant variation as the amplitude increases ($10\sim 60\%$). Compared to E , P_ζ in Fig. 5b features larger variations. With 0.1cm perturbation, the variation is not significant ($\sim 2\%$) but as the perturbation amplitude increases, the final P_ζ values vary more than 100% from the initial ones. This indicates that fast particles can be efficiently redistributed in phase space by a sawtooth crash with a sufficient amplitude. Note that the variation of P_ζ occurs mostly inside the sawtooth mixing radius around $P_\zeta = -0.5$ in this case, which depends on energy and pitch (ratio of parallel to total velocity). Although the variation is not significant, E is not conserved due to the finite electrostatic potential and mode frequency. The perturbation brings a perturbed electric field that results in the change in E , but due to low mode frequency the variation of E is small relative to that of P_ζ . Based on this results, further analysis focusing on the fast particle redistribution in phase space will be discussed for a fixed mode amplitude $\xi_0 = 7.5\text{cm}$.

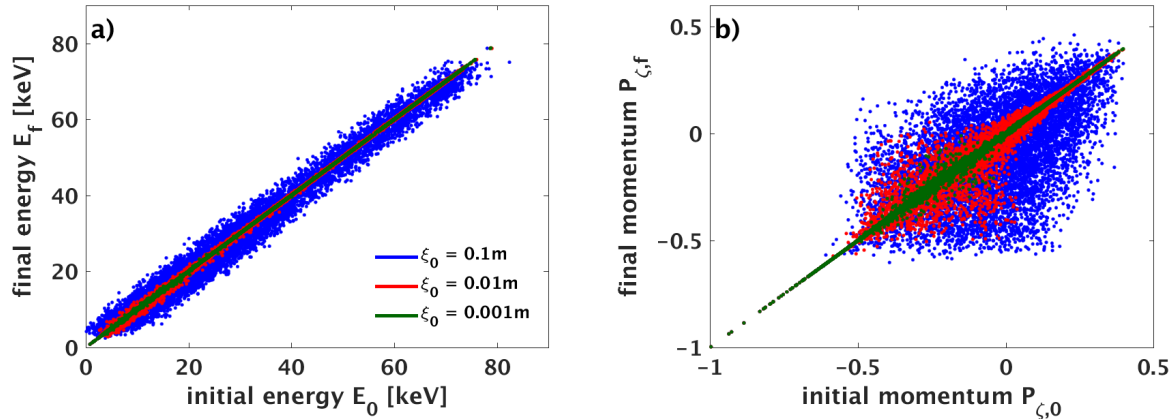


Figure 5: a) Fast particle energy E and b) canonical angular momentum P_ζ variations are shown for three different perturbation mode amplitude (blue, red and green for $\xi_0 = 10, 1, 0.1\text{cm}$ cases, respectively). Energy does not change while momentum shows significant variation with larger amplitude.

In order to find the characteristics of fast particle redistribution, orbit type classification of each particle is carried out first. The classification allows to identify the characteristic particle transport of each orbit type and the change of orbit type due to sawtooth. Based on the initial energy and pitch angle, the orbit types of each particle are classified using the Hamiltonian equation of motion and conservation of canonical angular momentum P_ζ [23]

$$\begin{aligned} E &= \rho_{\parallel}^2 B^2 / 2 + \mu B + \Phi \\ P_\zeta &= g \rho_{\parallel} - \psi_p \end{aligned} \quad (5)$$

where $\rho_{\parallel} = v_{\parallel} / B$ the normalized parallel gyro radius, B the equilibrium magnetic field, $\mu = v_{\perp}^2 / (2B)$ the magnetic moment, Φ the electrostatic potential, g the poloidal current function and ψ_p the poloidal magnetic flux. Using Eq. (5), the boundary of each particle type can be defined for a given particle energy (see Fig. 7). An example of classified orbit trajectories of particles with similar energy ($\sim 40\text{keV}$) are shown in Fig. 6. The trajectory of co-passing particle, moving around the magnetic axis (black cross) in the same direction to the plasma current, is displayed in blue and the particle moving in the opposite direction (counter-passing particle) is shown in yellow. Green, light green and violet lines indicate trapped, stagnation and potato particles, respectively. The last closed flux surface and NSTX-U

limiter are shown in black dashed and solid lines. Note that these trajectories are obtained without perturbation and only confined particles are considered, i.e. lost particles are not displayed.

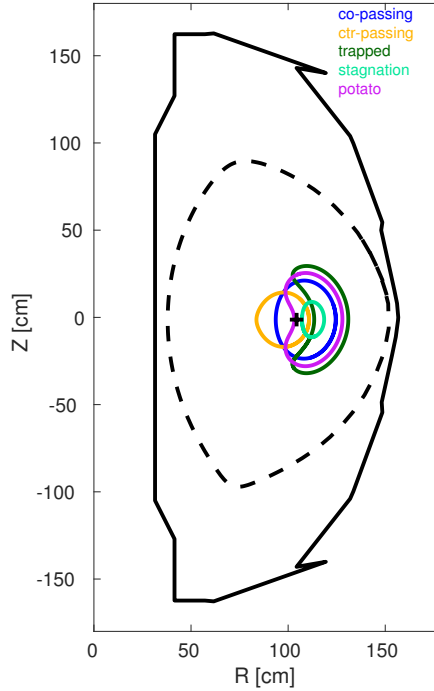


Figure 6: Trajectories of co-passing (blue), counter-passing (yellow), trapped (green), stagnation (light green) and potato (violet) types of particles with similar energy level of 40keV. The black solid and dashed lines indicate NSTX-U limiter and plasma boundary, respectively and the black cross sign is the magnetic axis.

Using the classification of particle orbit types, fast particle distribution in phase space is presented in Fig. 7. The perturbation amplitude is set to $\xi_0 = 7.5\text{cm}$ and two different initial energy cases are shown. The upper figures show the fast particle distribution without and with perturbation (before and after sawtooth crash) for the low energy case (between [15, 25]keV), while the bottom ones refer to higher energy particles between [50, 70]keV. The horizontal axis is the angular momentum P_ζ normalized by the poloidal flux at the edge $\psi_{p,e}$ and the vertical one is the ratio of the magnetic moment to particle energy. For the case with perturbation, the initial orbit type is used for each particle thus one can track the redistribution of particles. The classification boundaries are shown in red dashed lines in each figure for the average energy, i.e. 20 and 60keV. For both initial energy cases, without perturbation particles with different orbit types are well localized within the orbit boundaries (the colors of particles for different orbit types are the same from Fig. 6). After a sawtooth crash, the orbit type is no longer consistent with the boundaries for some particles due to the redistribution. For example, stagnation particles (light green) are found outside trapped and co-passing particle boundaries but most of particles move inside trapped or co-passing particle boundaries, which means the particles' position in phase space and the orbit type are modified by the perturbation. The investigation of redistribution of fast particle in phase space and the change of orbit topology are important as they allows to see how particles with different orbit types are differently affected by sawtooth crash qualitatively and to better interpret/understand experimental data that show different behaviour for particles with different orbit types due to sawtooth [9].

Figure 7 shows the redistribution and orbit type change of fast particle in certain energy ranges. One can also find the change of orbit type quantitatively for all particles. Figure 8a shows the number of particles that change their orbit type during the sawtooth crash. Right and left axes are the initial and final orbit types and each block with number represents the number of particles with the given initial and final orbit type set. The orbit type numbers for confined particles are 1 for co-passing, 3

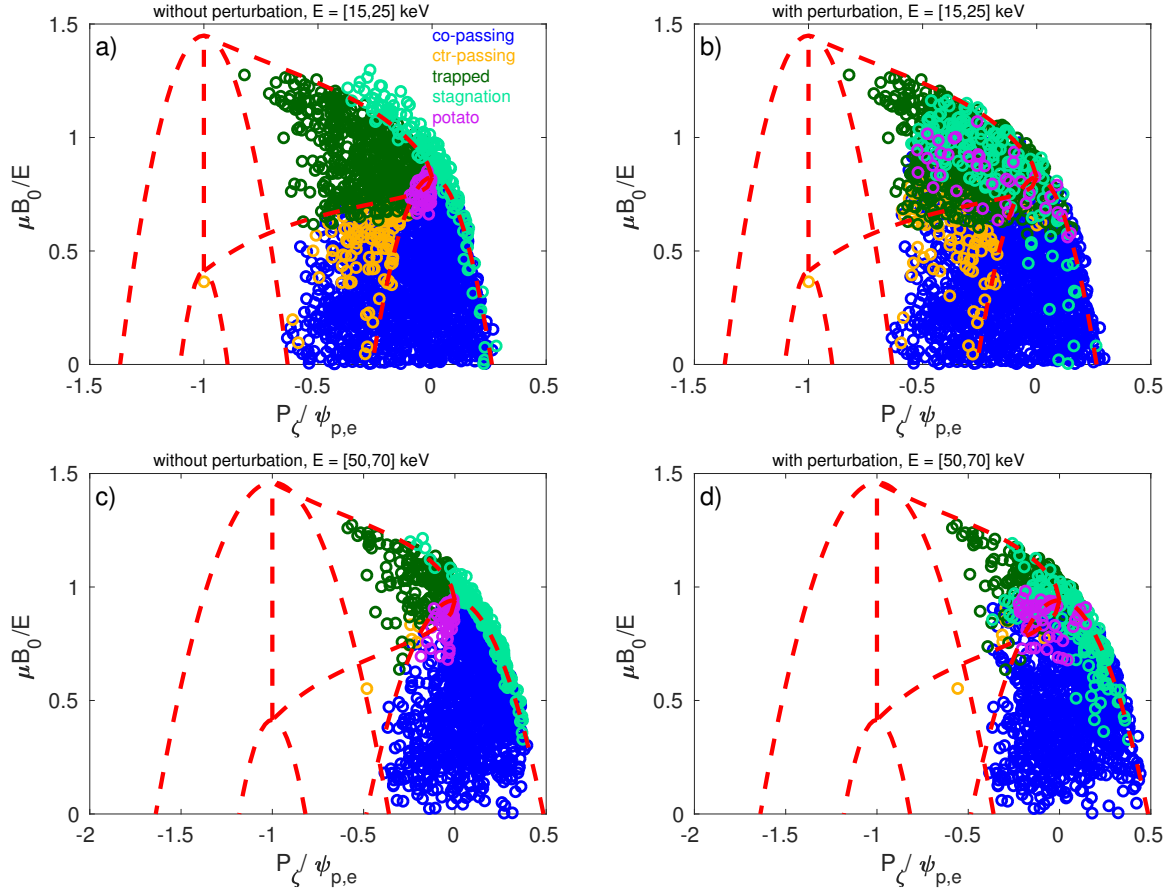


Figure 7: Fast particle distributions are shown for energy level of [15, 25]keV *a*) without and *b*) with perturbation and for higher energy level [50, 70]keV *c*) without and *d*) with perturbation. For both without and with perturbation cases, the initial orbit type is used to track the change of particle position and final orbit type. The orbit type boundaries, displayed as red dashed lines, are estimated using the average energy (20 and 60keV). Initially without perturbation, particles with each orbit type are well located in the boundaries but after the perturbation is applied, particles experience changes of position in phase space and the change of orbit type.

for counter-passing, 5 for trapped, 7 for stagnation and 8 for potato particles. For instance, initial and final orbit type set (1,5) and the corresponding number 556 mean that 556 initially co-passing particles turn into trapped particles after the crash. Among the 10,000 particles about 26% particles experience orbit type change and the largest changes are found from co-passing and stagnation to trapped particles. In addition, large portion of counter-passing and potato particles also turn into trapped particles while trapped particles mostly become co- or counter-passing particles. Note that in this figure the particles that keep their initial orbit types are not shown.

In Fig. 8b, the fraction of each orbit type after the crash is displayed versus the initial orbit type. As seen in Fig. 7, most of co-passing ($\sim 85\%$) and trapped ($\sim 77\%$) particles keep their initial orbit type while other types of particles have significant fractions of changed orbit type, mostly turning into trapped particles ($\sim 35\%$ of counter-passing, $\sim 60\%$ of stagnation, $\sim 53\%$ of potato particles). Stagnation and potato particles are located in just outside or between boundaries of different orbit types, thus it is easier to change their orbit type and the fraction of modified orbit type is much larger compared to passing and trapped particles. Note that only about 9% of co-passing particles become trapped particle after the crash. However the total number of co-passing particle is the largest and the 9% makes the similar number of change as stagnation case as shown in Fig. 8a.

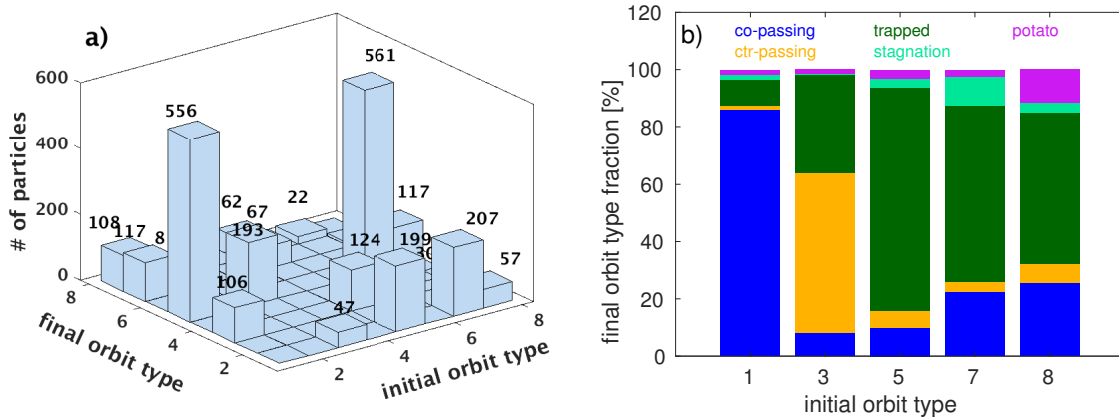


Figure 8: The change of orbit type after the sawtooth crash is quantitatively analysed as a) set of initial and final orbit type (i, f) and b) the fraction of each orbit type. $(i, f) = (1, 5)$ means initially co-passing particle turns into trapped particle after the crash. Most of case, particle orbits are converted to trapped particles while trapped particle becomes co- or counter-passing particles.

Similar to the effect of sawtooth crash on fast ion redistribution in phase space, the modification of fast ion distribution can also be seen in real space depending on the orbit type. The number of passing and trapped particles evaluated at each counting bin across the flux surfaces are shown in Fig. 9. To improve the statistics, the number of particle is accumulated over $10\mu\text{s}$ with zero perturbation amplitude to complete a few orbits before and after a sawtooth crash. Figures 9a and b show the initial (blue circle) and final (red cross) number of particles at each counting bin for co- and counter-passing particles while that of trapped particles is depicted in Fig. 9c. Note that particles are classified based on their initial orbit type for both initial and final profiles, so that those figures show the redistribution of the initial types of particles in real space regardless the final orbit type.

Co- and counter-passing particles are centrally peaked before crash and due to the perturbation, centrally located particles move outside the $q = 1$ surface (black dashed line) after crash. The final status of co- and counter-passing particle show clear effect of sawtooth instability. However, trapped particles show different behaviour compared to passing particles. Initially trapped particles have broader profile and hollow region in the center. After the crash, the profile is modified but sawtooth induced redistribution outside the $q = 1$ surface is not clearly seen as for passing particles.

The simulation results show that passing particles are more significantly affected by sawtooth instability than trapped particles. One likely explanation is the dependence of the redistribution process on fast ion energy. Based on the criteria for sawtooth induced redistribution [12], the critical initial energies of passing and trapped particles for redistribution are evaluated for this discharge. The critical energy for passing particles varies depending on the particles' pitch and can be $60\sim 70\text{keV}$ to a few hundred keV while about 30keV for trapped particles. The minimum and maximum particle energies are about

10 and 100keV. Therefore, most of passing particles are under the effect of sawtooth to be redistributed whereas only trapped particles that have energy similar or lower than 30keV are mostly affected.

These results are qualitatively consistent with experimental observation from a similar NSTX-U discharge, cf. Ref. [9]. As already mentioned, the effects of sawtooth on different orbit type are not taken into consideration in the current sawtooth model in TRANSP when the model is applied to fast ion redistribution. Therefore, even if TRANSP simulation can reproduce experimental neutron rates using an *ad-hoc* set of free parameter, the details of the fast ion distribution evolution can be different. For instance, the experimental measurement of fast ion profiles from FIDA system mostly sensitive to co-passing fast ions shows a clear effect of sawtooth, while the FIDA simulation result based on TRANSP simulations that reproduce the experimental neutron rate is not consistent with the measurement and the effect of sawtooth around the inversion radius is not clear [9].

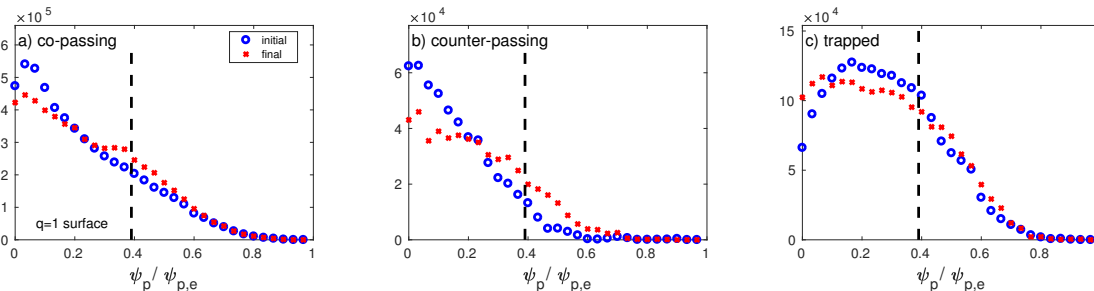


Figure 9: Number of particle at each counting bin before (blue circle) and after (red cross) sawtooth crash for *a*) co-passing, *b*) counter-passing and *c*) trapped particles. Passing particles show clear redistribution induced by sawtooth while the final state of trapped particles does not give a clear sign of sawtooth effect. The sawtooth inversion radius for passing particles is located near $\psi_p/\psi_{p,e} \sim 0.25$.

The ORBIT results discussed previously indicate that energetic particle (EP) transport by sawteeth has complicated dependencies on the EP phase space variables, which cannot be represented through a simple, zero-dimensional analysis. Referring to future burning plasmas, the EP distribution function is expected to be a complicated function of phase space, with fast ions from alpha reactions, NB injection and - possibly - RF waves in the ion cyclotron range of frequency. Therefore, it seems likely that a comprehensive EP transport model must have phase space resolution to correctly recover the effects of sawteeth.

To test this idea, the reduced *kick model* [14, 15] for fast ion transport presently implemented in TRANSP is used in conjunction with results from the ORBIT modeling. The kick model is based on ‘transport probability matrices’ to represent EP transport by instabilities in the Monte-Carlo NUBEAM module of TRANSP. The matrices are computed from either numerical simulations (e.g. through ORBIT) or theory. In essence, each matrix represents the probability that fast ions from a certain (E, P_ζ, μ) region in phase space (where μ is the magnetic moment) will experience changes - or *kicks* - in energy and P_ζ by an instability during their orbiting over a certain time interval. For this work, the same ORBIT framework discussed above is used to compute a probability matrix associated with the sawtooth.

As discussed in Sec. 2, the experimental data available for the sawtooth L-mode scenario during the NSTX-U commissioning phase present large uncertainties. Therefore, these initial TRANSP simulations should be intended as an exploratory work rather than as a detailed, quantitative analysis of the actual experiment. For example, simulations shown in Fig. 10*b* indicate that most of the drop in the measured neutron rate may actually be caused by sawtooth-induced changes in the thermal plasma profiles. Simulations that include the reconstructed profiles, but do not evolve the fast ion population, achieve neutron rate drops that are (on average) comparable to the measured ones.

Nevertheless, the simulation results also show potential from improvement of the sawtooth models presently implemented in TRANSP. Figure 10*a* shows the evolution of the NB ion density profile from TRANSP simulations using the kick model to mimic sawtooth effects on NB ions. One main conclusion is that the kick model can recover the increase of NB ion density across the inversion radius as seen in Fig. 10*c*. This, not present in simulations using the standard sawtooth models in TRANSP, is consistent with experimental observations from FIDA [9] and seems to suggest that the kick model can recover features not included in the present models.

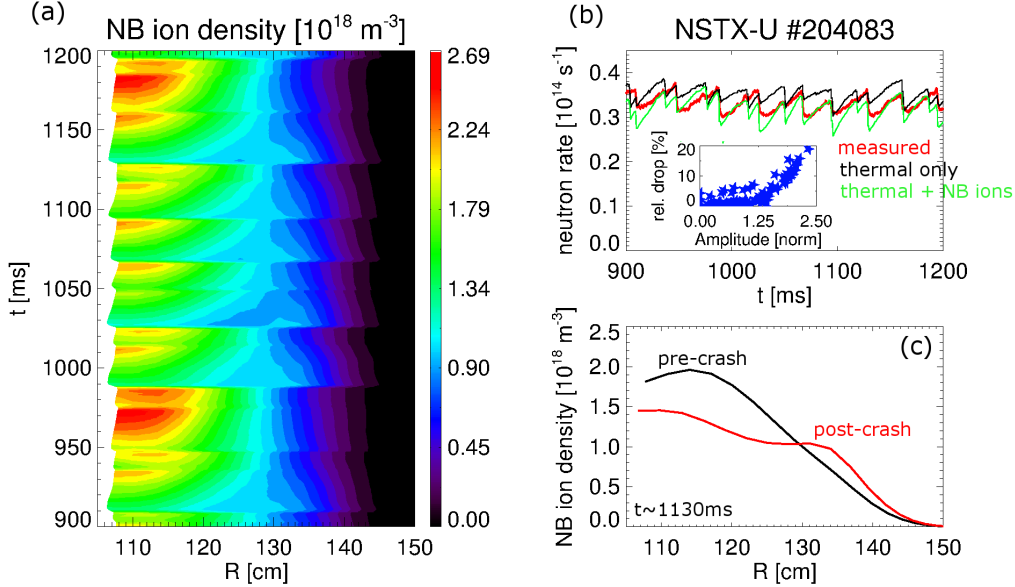


Figure 10: *a*) NB ion density evolution vs time and radius. *b*) Measured neutron rate (red) compared with TRANSP results that include variations of thermal profiles only (black) and of thermal plus NB ion profiles (Green). The inset shows the contribution to the relative drop in neutron rate caused by NB ion transport as the amplitude of the sawtooth events is increased in the simulation. *c*) NB ion density profiles from TRANSP just before and after a sawtooth crash. Note the formation of a ‘shoulder’ across the inversion radius, $R \approx 130 \text{ cm}$, which reminds the experimental observations from FIDA for co-passing fast ions [9].

4 Conclusion

Modeling of sawtooth discharge helps to understand/interpret experimental results and to set an operation scenario with prediction of behaviour of sawtooth instability. In order for the sawtooth modeling to provide more reliable prediction, the characteristics of fast ion transport should be taken into consideration. As the first step of the development of a comprehensive model for fast ion transport induced by sawtooth crash, modeling using the ORBIT code is performed based on a NSTX-U sawtooth discharge to find the effect of sawtooth instability on fast ion redistribution depends on the characteristics of fast ions such as energy, angular momentum, magnetic moment and pitch angle.

Sawtooth instability can be applied to the ORBIT code by implementing linear plasma displacement as the displacement induces perturbed magnetic fields. The normalized radial profile of the given displacement is modified to have zero amplitude at the magnetic axis to avoid an intrinsic numerical problem of the ORBIT code. The normalized temporal profile is defined with characteristic times of NSTX-U sawtooth discharges. The maximum amplitude of the displacement is determined by the comparison with experimental measurement of neutron rate. Since the ORBIT code does not provide direct calculation of neutron rate, the relative change of neutron rate before and after sawtooth crash is used for the comparison.

The effect of sawtooth crash is investigated in phase space for different fast ion orbit types. Due to the application of perturbation, both energy and canonical angular momentum of fast ion are not conserved although the change of particle energy before and after a sawtooth crash is not significant. With a sufficiently large perturbation amplitude, particles are redistributed by sawtooth in phase space. Orbit types are also modified. Most of co-passing and trapped particles keep their orbit type while large fraction of counter-passing, stagnation and potato particles turn into trapped particles due to the perturbation.

The redistribution of fast ions in real space indicates that passing particles are more affected by sawtooth than trapped particles. The number of co- and counter-passing particles at each counting bin show the clear effect of sawtooth crash, the centrally located particles move out after the crash. Trapped particles distribution is also modified by sawtooth crash but the result is opposite to passing particle case.

The different behaviour of passing and trapped particles are qualitatively consistent with the experimental measurements. This might be because of the different critical energies from the criteria for sawtooth induced redistribution [12]. For the conditions investigated in this work, passing particles have a critical energy 60keV or larger depending on particles' pitch angle, thus most particles are affected by sawtooth. Fewer trapped particles are influenced as their critical energy is about 30keV. The criteria introduced in a theoretical work can be useful to compare with simulation results and to find characteristics of fast ion transport during sawtooth crash. Therefore, more effective way to compare with the theory need to be applied as well as an improved sawtooth modeling that includes more physics and is more reliable is required beyond simple zero-dimensional prediction.

The initial TRANSP simulation result that applies kick model combined with the ORBIT modeling shows potential improvement of the present sawtooth model. Although the neutron rate is in disagreement with the measurement, the NB ion density after a crash is consistent with the FIDA data. The latter cannot be seen using the present sawtooth model. Clearly, more work is required to explore the potential of the kick model (or a derived version of it) for improvements over the existing sawtooth models in TRANSP. To overcome the limitations of diagnostic data from the NSTX-U commissioning campaign, diagnostic improvements are under way for kinetic profile diagnostics in view of the next NSTX-U campaign. Upgrades to the CHERS system will result in a four-fold reduction in sampling rate, thus allowing a 2.5ms time resolution for full radial profiles of ion density, temperature and toroidal rotation. A new pulsed Thomson scattering system is being installed to achieve a time resolution ≤ 1 ms for electron density and temperature. In the short term, data from other devices would also prove useful for further model validation and development.

Acknowledgements

Work supported by the U.S. Department of Energy, Office of Science, Office of Fusion Energy Sciences under contract number DE-AC02-09CH11466.

References

- [1] F. Porcelli, Boucher D., and Rosenbluth M.N. *Plasma Phys. Control. Fusion*, 38:2163, 1996.
- [2] O. Sauter et al. *Phys. Rev. Lett.*, 88(10):105001, 2002.
- [3] M. Ono et al. *Nucl. Fusion*, 40:557, 2000.
- [4] J.E. Menard et al. *Nucl. Fusion*, 52:083015, 2012.
- [5] J.E. Menard et al. *Nucl. Fusion*, 57:102006, 2017.
- [6] R.J. Hawryluk. *An empirical approach to tokamak transport Physics Close to Thermonuclear Conditions vol 1 ed B. Coppi et al (Brussels: Commission of the European Communities) p 19.* 1980.
- [7] For more details on the TRANSP code, please refer to the TRANSP webpage at <http://w3.pppl.gov/~pshare/help/transp.htm>.
- [8] B. Kadomtsev. *Soviet Journal of Plasma Physics*, 1:710, 1975.
- [9] D. Liu et al. *15th IAEA-TM EP meeting (Princeton, NJ - USA, 2017), submitted to Nucl. Fusion.*
- [10] A. Bortolon, W.W. Heidbrink, and M. Podestà. *Rev. Sci. Instrum.*, 81:10D728, 2010.
- [11] M. Podestà, W.W. Heidbrink, R.E. Bell, and R. Feder. *Rev. Sci. Instrum.*, 79:10E521, 2008.
- [12] Ya. I. Kolesnichenko, V.V. Lutsenko, and Yu. V. Yakovenko. *Phys. Plasmas*, 4:2544, 1997.
- [13] R.B. White and Chance M.S. *Phys. Fluids*, 27:2455, 1984.
- [14] M. Podestà, M. Gorelenkova, and R.B. White. *Plasma Phys. Control. Fusion*, 56:055003, 2014.
- [15] M. Podestà, M. Gorelenkova, N.N. Gorelenkov, and R.B. White. *Plasma Phys. Control. Fusion*, 59:095008, 2017.
- [16] B.P. LeBlanc. *Rev. Sci. Instrum.*, 79:10E737, 2008.

- [17] R.E. Bell et al. *Phys. Plasmas*, 17:082507, 2010.
- [18] R.J. Goldston et al. *J. Comput. Phys.*, 43:61, 1981.
- [19] A. Pankin et al. *Computer Physics Communication*, 159:157, 2004.
- [20] R. Farengo et al. *Nucl. Fusion*, 53:043012, 2013.
- [21] Yi. Zhao and R.B. White. *Phys. Plasmas*, 4:1103, 1997.
- [22] R.B. White. *Phys. Plasmas*, 20:022105, 2013.
- [23] R.B. White. *The Theory of Toroidally Confined Plasmas*. Imperial College Press, 3rd edition, 2014.